HHS Public Access

Author manuscript

Neuron. Author manuscript; available in PMC 2020 June 02.

Published in final edited form as:

Neuron. 2020 March 18; 105(6): 1018–1026.e4. doi:10.1016/j.neuron.2019.12.029.

A role for the locus coeruleus in hippocampal CA1 place cell reorganization during spatial reward learning

A.M. Kaufman[*,1,2,3,4], **T. Geiller**[*,1,2,3], **A. Losonczy**[1,2,3]

[1]Department of Neuroscience, Columbia University, New York, NY 10027, USA

[2]Mortimer B. Zuckerman Mind Brain Behavior Institute, Columbia University, New York, NY 10027, USA

[3]Kavli Institute for Brain Science, Columbia University, New York, NY, USA

[4]Graduate program in Neurobiology and Behavior, Columbia University, New York, NY 10027, USA

Summary

During spatial learning, hippocampal (HPC) place maps reorganize to represent new goal locations, but little is known about the circuit mechanisms facilitating these changes. Here, we examined how neuromodulation via locus coeruleus (LC)- projections to HPC area CA1 (LC-CA1) regulates the overrepresentation of CA1 place cells near rewarded locations. Using two-photon calcium imaging, we monitored the activity of LC-CA1 fibers in the mouse dorsal HPC. We find that the LC-CA1 projection signals the translocation of a reward, predicting behavioral performance on a goal-oriented spatial learning task. Optogenetic stimulation mimicking this LC-CA1 activity induces place cell reorganization around a familiar reward, while its inhibition decreases the degree of overrepresentation around a translocated reward. Our results show that LC acts in conjunction with other factors to induce goal-directed reorganization of HPC representations, and provide a better understanding of the role of neuromodulatory actions on HPC place map plasticity.

Introduction

The concept of a ‘cognitive map’, a mental representation of the world, has long been part of neuroscience (Tolman, 1948). A subset of principal neurons in the hippocampus (HPC) are active at specific locations in an environment (‘place cells’, O’Keefe and Dostrovky, 1971), suggesting that the HPC may provide a neural substrate for cognitive maps (O’Keefe and Nadel, 1978). To maintain behaviorally relevant representations, HPC place cell maps flexibly reconfigure during behavioral tasks with specific cognitive demands (Colgin et al., 2008). This phenomenon is demonstrated during goal-oriented spatial learning tasks (Morris

Lead contact: Attila Losonczy – al2856@columbia.edu.

*these authors contributed equally

Author contributions

All authors designed the experiments. A.M.K. and T.G. collected and analyzed the data. All authors wrote the manuscript.

Declaration of Interests

The authors have no competing interests related to this work.

et al., 1982), where place cells overrepresent rewarded locations upon learning (Danielson et al., 2016; Dupret et al., 2010; Hollup et al., 2001; Turi et al., 2019; Xu et al., 2019; Zaremba et al., 2017). However, the circuit mechanisms underlying this plasticity remain poorly understood.

HPC circuit dynamics are under neuromodulatory control from subcortical nuclei (Palacios-filardo and Mellor, 2019). Among these, the brainstem locus coeruleus (LC) (Sara and Bouret, 2012) is a major source of catecholamines in the HPC (Smith and Greene, 2012), releasing both noradrenaline (NA) and dopamine (DA). The LC has long been known for its involvement in cognitive flexibility and orienting toward salient stimuli (Foote et al., 1983). More recently, LC activity has been demonstrated to accelerate perceptual (Glennon et al., 2019; Martins and Froemke, 2015) and spatial learning (Kempadoo et al., 2016; Takeuchi et al., 2016).

Given the rich literature on the effects of catecholamines on HPC plasticity and learning (Retailleau and Boraud, 2014), we investigated the activity of LC axons projecting to HPC CA1 area (LC-CA1) in a goal-oriented learning (GOL) task and tested their contribution to the reorganization of CA1 place cells. We found that LC-CA1 projections exhibited increased activity near a new reward location. Optogenetic activation of LC-CA1 axons near the reward induced place cell overrepresentation of a familiar rewarded location, enhancing reward-related place cell plasticity, while optogenetic inhibition of LC-CA1 axons suppressed place cell overrepresentation. In contrast, in a random foraging task where animals did not learn goal locations, LC-CA1 activation had no effect, and neither did conjunctive activation of multiple reward-related circuits, indicating a task-dependent nature for this mechanism. We conclude that the LC is a key player in inducing place cell reorganization, and that it likely acts in conjunction with other factors that are differentially active near rewards.

Results

In order to assess place cell dynamics during GOL, we virally expressed GCaMP6f in dorsal CA1, and implanted a cannula-window over dorsal CA1. Under the two-photon (2p) microscope, head-fixed mice performed the GOL task on a 2-meter treadmill belt containing tactile cues (Figure 1A, Methods). During GOL, an operantly delivered water reward was given in one location for three days (Reward Zone 1, RZ1), and was then moved to a second location for the last three days (Reward Zone 2, RZ2, Figure 1A) (Danielson et al., 2016; Turi et al., 2019; Zaremba et al., 2017). Learning was assessed by the proportion of licks in the reward zone (Figure 1B,C). CA1 pyramidal cells (CA1PCs) were imaged, and a subset of these was determined to be place cells based upon their spatial tuning (Fig. 1D, Methods). Similar to previous studies showing that place cells become enriched around a new, translocated reward location (Danielson et al., 2016; Turi et al., 2019; Zaremba et al., 2017), we found that reward overrepresentation was absent at RZ1, and pronounced in the last session of RZ2 (Figure 1E,F). We hypothesized that this enrichment could be caused by differential activity of LC-CA1 projections around the translocated reward.

To assess the activity of LC-CA1 projections, we virally expressed GCaMP6s in tyrosine hydroxylase (Th)-positive LC neurons (Figure 2A), and tracked the same LC-CA1 fibers during the GOL task (Figure 2B). LC-CA1 activity in each field of view was highly synchronous, with a small subset of inactive fibers (Figure S1, Methods). We first determined how different behavioral variables contributed to LC-CA1 activity during GOL using a generalized linear model (GLM) (Figure 1C,D, Methods). We computed the cross-validated coefficient of determination R^2 on the held-out test data (Figure 2C), and observed that R^2 values were higher in the RZ2 than RZ1 phase of the task (Figure 2D). To determine the contribution of the different variables in each task phase, we computed the log-likelihood ratio between the full and reduced models, in which a given variable was omitted (Figure S1H,I, Methods), and found that the contribution of position significantly increased in the RZ2 task phase (Figure 2D). We reasoned that the increase was due to differences in LC-CA1 activity at specific locations, and so we decided to examine LC-CA1 calcium signals around each RZ.

When the mouse approached RZ1, the LC-CA1 signal rose and fell with velocity (Figure 2E,F). After reward translocation, when the mouse approached RZ2, LC-CA1 activity was less correlated with velocity, manifested in a dip, followed by an overshoot (Figure 2E,F). This overshoot preceded the reward, and developed on the first day of RZ2 (Figure S2A), consistent with a predictive reward signal (Bouret and Sara, 2004). We did not see an LC-CA1 response near the old reward zone after the reward was moved, nor did we see an increased LC-CA1 response near the new reward zone before it was moved (Figure S2B). We quantified the degree of the overshoot using a linear regression between the velocity and the axonal calcium signal just before the reward onset (Methods), and found that LC-CA1 activity became gradually decorrelated from velocity after the RZ was moved (Figure 2G, Methods). The less LC-CA1 activity was correlated with velocity, the better the mice performed on the task (Figure 2H), and in mice that did not learn the second reward location, LC-CA1 activity remained correlated with velocity (Figure 2G, non-learning). The decorrelation from velocity began in the first few sessions of RZ2, while in RZ1, velocity and the LC-CA1 signal remained correlated (Figure S2C). The correlation began to decrease even during the first few laps of the first session, decreasing during the first few laps each day (Figure S2D), while place cell enrichment gradually increased across sessions after reward translocation (Figure S2E). Thus, the LC-CA1 signal begins before the place cell enrichment, and is maintained over time while enrichment increases (Figure S2E).

We found that this spatially localized increase in activity was not related to improved task performance (Figure S3A), as when we imaged LC-CA1 activity for six days without moving the reward, LC-CA1 activity did not develop an overshoot near the reward, and the correlation between velocity and LC-A1 activity increased over time (Figure S3B). We also imaged CA1PC activity during the second three days of RZ1, and enrichment did not occur at RZ1, even after six days. We then moved the reward, and observed place field enrichment around the translocated reward (Figure S3C). These results show that upon learning a new reward location, LC-CA1 axons develop a spatially localized increase in activity just before the new reward, and place cell reorganization and enrichment follows this increase (Figure 1E,F, Figure S2). Therefore, we next tested whether activation of LC-CA1 could generate reward-related enrichment of CA1PCs.

We used an all-optical system to simultaneously stimulate optogenetically and image through the cannula-window (Turi et al., 2019) (Figure 3A, Methods). We confirmed that we could activate LC-CA1 axons by co-expressing a red-shifted excitatory opsin (bReaChes) and GCaMP6s (Figure 3A–C) in LC-CA1 axons. Next, we simultaneously activated LC-CA1 axons with bReaChes and imaged CA1PCs with GCaMP6f (Figure 3D). Optogenetic activation of LC-CA1 axons did not acutely affect CA1PCs activity (Figure 3E).

Since both the overshoot of LC-CA1 activity and the enrichment of place cells occur around the translocated reward (RZ2), we next aimed to optogenetically recapitulate the LC-CA1-overshoot in the first phase of the task, near RZ1, where enrichment normally does not occur (Figure 1E,F). Using the LC-bReaChes, CA1PC-GCaMP strategy, we stimulated LC-CA1 fibers prior to the reward (Figure 3F, top). For analysis of place cell activity near reward, we included the area preceding the reward and spanning the entire RZ, hereafter referred to as the peri-reward zone (pRZ) (Figure 3F, top). This local, unilateral LC-CA1 stimulation, beginning partway through the task, did not alter behavioral performance (Figure 3F, bottom), or the properties of place cells in the pRZ (Figure 3D). Strikingly, however, we observed a robust enrichment of place cells near the reward in the last session that was not present in control animals (Figure 3G–H).

This enrichment could stem from recruitment of *de-novo* place cells, or a shift of place fields toward the reward. To determine the source of the enrichment, we looked at the place cells in the pRZ during the last session, and examined their recurrence probability in previous sessions (Zaremba et al., 2017). We observed similar recurrence dynamics between experimental and control groups, indicating that LC-CA1 activation likely did not induce new place fields (Figure S3E). In the experimental group, some place cells in the pRZ in the last session were active outside the pRZ in sessions before LC-CA1 stimulation (Figure S3F). In addition, place cells that were inside the pRZ after LC-CA1 stimulation were more stable than place cells outside it (Figure S3G) Thus, LC-CA1 activation shifts existing place cells toward the reward, and stabilizes place cells around the reward.

We next sought to determine whether LC-CA1 activity was necessary for place cell enrichment normally observed around the translocated reward. We used an LC-archaerhodopsin (ArchT), CA1PC-GCaMP strategy to inhibit LC-CA1 activity around RZ2 (Figure 4A,B), and imaged CA1PCs during the last session. As with excitation, local, unilateral inhibition of LC-CA1 fibers did not affect behavioral performance (Figure 4C). However, inhibiting the LC-CA1 axons near the second reward decreased the degree of place field enrichment (Figure 4D).

Next, we asked whether optogenetic activation of LC-CA1 fibers was sufficient to drive place cell overrepresentation when the stimulation was not paired with a reward location in three different paradigms. First, we stimulated in an unrewarded area during the first reward zone of the GOL task. This protocol produced no effect on the number of place cells in the stimulated area (Figure S4A,B). To test for putative interactive effects between stimulation and learning the zone, we next stimulated LC-CA1 axons in a constant location during a non-spatial task, where the animal is rewarded at randomized locations (random foraging, Danielson et al., 2016), and did not see enrichment around the stimulated zone (Figure 4C–

E). Lastly, we combined optogenetic LC-CA1 stimulation with addition of a novel cue on the belt, which also did not cause place field reorganization (Figure S4H).

Finally, we examined whether the LC-CA1 projection could act in conjunction with other reward-related HPC microcircuits to influence place cell plasticity. We have recently demonstrated that disinhibition conveyed by Vasoactive Intestinal Polypeptide (VIP)-expressing interneurons plays a role in regulating reward-related place cell representations (Turi et al., 2019). Therefore, we simultaneously stimulated CA1 VIP interneurons and LC-CA1 axons (Figure S4F) at a constant location during the random foraging task, to decouple stimulation from reward. This combined stimulation did not lead to place cell shift toward the stimulated site (Figure S4G). Since LC-CA1 stimulation caused place field enrichment only at a rewarded site, and only during a learning task, we conclude that LC inputs to CA1 acts in conjunction with other signals that occur around rewards in a task-dependent manner.

Discussion

It has been suggested that CA1PCs are equally competent to become place cells (Bittner et al., 2017, 2015), implying that all cells receive the requisite inputs for all locations, and thus could remap or stabilize when the cell's response to a specific input is altered. Our data show that LC-CA1 activity increases before reward delivery, which, together with evidence of place cell enrichment before the reward zone, may indicate the opening of a plasticity window for the potentiation of inputs that predict rewards (Stachenfeld et al., 2017). Optogenetic stimulation mimicking this change in LC-CA1 activity induced goal-directed reorganization of place cells, but only near a reward, primarily through a goal-directed shift toward and stabilization of place cells.

The structure of the GOL task in this study was such that when the mouse was first exposed to RZ1, the context was novel. Other studies examining goal-directed reorganization were performed in a familiar environment – changes in reward representation tend to occur when patterns of reinforcement change (Breese et al., 1989; Dupret et al., 2010; Fyhn et al., 2002; Hok et al., 2007; Hollup et al., 2001; Kobayashi et al., 1997). Therefore, one explanation for place cell enrichment occurring in RZ2, rather than RZ1, is that goal-directed place cell dynamics are obscured by conflicting demands related to the formation of stable contextual representations. Once a stable representation is established, changes could result in goal-related overrepresentation of place cells. A recent study described "reward cells" that track rewarded locations (Gauthier and Tank, 2018), which we did not investigate here, because the reward was moved only once in our task. Reward-related enrichment was not explicitly described in recent studies imaging CA1PCs in a familiar environment (Dombeck et al., 2010; Hainmueller and Bartos, 2018; Ziv et al., 2013). This may be due to differences in task structure: our task is operant to ensure the mice learn the location, while to our best understanding the tasks in the referenced studies used non-operant reward, which may reduce learning demands.

The finding that LC-CA1 activity increases specifically near a new rewarded location is consistent with the LC playing a role in orienting toward unexpected stimuli (Aston-Jones and Waterhouse, 2016); these stimuli could be relevant for behavior, and merit

overrepresentation. Additionally, the time course of place cell reorganization was slower than that of the reward-related LC signal, perhaps due to offline consolidation that occurs between sessions or during sleep that may help the plasticity to peak.

The signaling mechanism for LC-activation induced place cell reorganization is unknown. Thus far, the major effects of the LC on HPC learning appear to be mediated through D1/D5 DA receptors, and not through β-adrenergic receptors (Kempadoo et al., 2016; Takeuchi et al., 2016), although α1 receptors can accelerate perceptual learning (Glennon et al., 2019). Thus, NA, DA, or both could be responsible for both the native and induced enrichment we observed. Future experiments could determine the source of the enrichment by blocking these receptors.

To avoid spurious changes to HPC representations, simultaneous engagement of multiple systems may be required. Consistent with this, LC-CA1 stimulation only drove place cell enrichment when paired with a rewarded location. This could also explain why neither local, unilateral LC-CA1 activation or inhibition led to a behavioral effect. Some factors known to be differentially active for reward learning include disinhibitory circuits (Turi et al., 2019) and other neuromodulatory transmitter actions, such as serotonergic (Teixeira et al., 2018) and cholinergic activity (Hangya et al., 2015; Palacios-filardo and Mellor, 2019). In addition, the ventral tegmental area (VTA) may act together with the LC to influence place cell plasticity, possibly during different brain states (Duszkiewicz et al., 2019; Gomperts et al., 2015; McNamara et al., 2014). Other cellular participants in neural transmission, such as astrocytes, could also be involved (Bazargani and Attwell, 2016).

Coactivation of LC-CA1 stimulation with VIP interneuron-mediated disinhibition did not lead to place cell enrichment in a random foraging task, suggesting either that VIP interneurons and the LC do not work together, or that place cell plasticity depends on the cognitive load of the task. Task-related demands affect the stability of HPC representations in a DA-dependent manner (Kentros et al., 2004). We found that LC-CA1 stimulation outside the reward location, even in a GOL task, did not induce place cell reorganization. The parsimonious explanation for these results may be that task demands lead to a higher baseline neuromodulatory tone, upon which multiple reward-related systems, including the LC, can act to induce plasticity.

High baseline LC-CA1 activity may increase place cell stability during their formation by altering the NAergic or DAergic tone, creating a favorable state for CA1PCs to strengthen their responses to inputs. Indeed, the LC is highly active in novel environments (Takeuchi et al., 2016), and inhibiting LC-CA1 axons during initial context exposure prevents contextual learning and causes CA3 place cells to become unstable upon re-exposure to a familiar environment (Wagatsuma et al., 2018). Thus, our results are compatible with a role for the LC in adjusting, strengthening, or altering the responses of CA1PCs to their inputs.

High neuromodulatory activity seems to be a trademark signal during locomotion and arousal. For example, the activity of some DAergic and cholinergic axons are found to be correlated with movement, reward (Howe and Dombeck, 2016) and changes in movement state (Howe et al., 2019), and LC axonal activity in the cortex is correlated with pupil

dilation, which is correlated with movement (Breton-Provencher and Sur, 2019). While we see initially that the LC is correlated with movement, its relationship with velocity changes once the learning paradigm changes. Future experiments could determine if other neuromodulatory projections also exhibit learning related changes.

Our results support a working model where a balance of differential neuromodulatory, local inhibitory and astrocyte calcium activity that act on top of task-related brain states to alter the HPC cognitive map. We found that LC-CA1 stimulation could tip the balance toward place cell reorganization when other components were in place due to the presence of a reward. Future studies can untangle the precise identities of these ingredients and how they interact with each other, but our findings show that the LC is a key player in HPC population dynamics supporting goal-directed learning.

STAR METHODS

LEAD CONTACT AND MATERIALS AVAILABILITY

Further information and requests for resources and reagents should be directed to the Lead Contact Attila Losonczy (al2856@columbia.edu). All unique/stable reagents generated in this study are available from the Lead Contact with a completed Materials Transfer Agreement.

EXPERIMENTAL MODEL AND SUBJECT DETAILS

Experiments were conducted in accordance with NIH guidelines and with the approval of the Columbia University Institutional Animal Care and Use Committee. Experiments were conducted with male and female mice, age 2–4 months, on a C57BL/6J background. LC injections were performed in Th-IRES-Cre mice (obtained from Dr. Eric Kandel's laboratory at Columbia University) (Lindeberg et al., 2004), and Cre-negative littermates or wild-type mice. VIP-IRES-Cre mice were crossed to C57BL/6J mice, and then crossed with Th-IRES-Cre mice, which were on a C57BL/6J background.

METHOD DETAILS

Viruses—Recombinant adeno-associated viruses (rAAVs) were used for GCaMP6 and optogenetic channel expression. Cre-dependent bReaChes (Rajasethupathy et al., 2015), a red-excitation shifted variant of channelrhodopsin, expression was achieved with rAAV2/9:Ef1a-(bReaChes-tdTomato)^{Cre} (obtained from Dr. Boris Zemelman, UT Texas, Austin), GCaMP6s expression in the LC with rAAV 2/9:Ef1a-(GCaMP6s)^{Cre} (Dr. Boris Zemelman, UT Texas, Austin). For expression in CA1PCs, rAAV2/1:hSyn-GCaMP6f and rAAV2/1:CaMKII-GCaMP6f were used (see Key Resources Table). For experiments with viral mixtures, viruses were mixed in a 1:1 ratio. If animals were used for multiple experiments, they were trained on a burlap belt between paradigms.

Viral injection and hippocampal window/headpost implant—Viral injections were performed with a Nanoject syringe, as previously described (Lovett-Barron et al., 2014). Briefly, mice were anesthetized with isoflurane and treated with buprenorphine or meloxicam to minimize postoperative discomfort. The skull was exposed and a hole was

drilled, and a sterile glass capillary containing viral mixtures was lowered into the brain. After injections, the skin was sutured and mice were allowed to recover. The LC was injected bilaterally at coordinates AP −5.45 mm, ML ±1.28 mm, and DV −3.65 mm with 150 – 300 nL of virus. The dorsal HPC area CA1 was injected in the left hemisphere at coordinates from Bregma AP −2.1 or −2.2, ML −1.5 or −1.75, and DV −1.2, −1.1, and −1.0 with 50–64 nL of virus at each DV site. Mice were implanted with an imaging window (diameter 3.0 mm, height 1.5 mm) over the left dorsal-intermediate hippocampus with a stainless-steel or brass headpost. Imaging cannulas were constructed by adhering (Norland optical adhesive) a 3-mm glass coverslip (64–0720, Warner) to the steel cannula (Ziggy's tubes and wires). The surgical procedure has been described previously (Lovett-Barron et al., 2014). Briefly, mice were anesthetized and treated with buprenorphine or meloxicam, the skull was exposed and a 3 mm hole was made in the skull. Bone, dura and cortical layers were removed, while flushing with ice-cold cortex buffer. The cannula was inserted into the hole, secured with Vetbond, and a headpost was affixed to the skull with dental cement. Mice recovered in their home cage, and were monitored for three days post-surgery.

***In vivo* calcium two-photon imaging and optogenetics—**Imaging was conducted using a two-photon 8 kHz resonant scanner (Bruker). A piezoelectric crystal was coupled to the objective as described previously (Danielson et al., 2016) in order to allow fast displacement along the Z-axis. The objective was a Nikon 40x NIR water immersion, 0.8 NA, 3.5 mm working distance. The excitation laser was 920 nm (50–100 mW, Coherent Ultra II). For some structural images in red, the laser was 1070 nm (Coherent Fidelity), and scanning was interlaced with the 920 nm laser for green excitation. Red (tdTomato) and green (GCaMP6) channels were separated by emission cubes as described previously (Danielson et al., 2016). Fluorescence signals were collected using photon multiplier tubes (PMT, GaAsP PMT, Hamamatsu R3896). A preamp (1.4 × 105 dB, Bruker) was used to amplify signals before digitization. Pockels cells were used to regulate the power of the LED reaching the tissue. Images were acquired at 1x digital zoom, 1.2, or 1.4, with 512 × 512 pixels. For CA1PCs, two separate planes were acquired from 20 μm and up to 30 μm apart, with the piezo waiting to settle at each plane for 35ms, such that the frame rate was about 8 Hz. For axons, 2–5 planes 2 μm apart were acquired to maintain the axon in the z plane.

For optogenetic experiments, a dichroic mirror was used to allow red light to pass through into the brain, and green light to be reflected into the PMT. The stimulation was performed with an ultrafast and high-power collimated LED, at 625 nm (Prizmatix, 625 nm). It was triggered using an Arduino board that gated the inverse photostimulation signal of the Pockels cell, which turns off briefly between mirror turnaround, as well as when the piezo reverses direction. The average power of the LED was 35–70 mW measured under the objective. This approach allowed us to protect our PMTs from the high intensity illumination but still take the advantage of the fast, full frame resonant galvo scanning without losing frames during photostimulation.

Behavioral experiments—Mice were trained on a cue-free burlap belt. 3–4 days after the implantation surgery, they were water deprived. First, they were habituated to head fixation for several 10-minute sessions. Then they were allowed to lick freely for water, which was

delivered initially at 15 locations on the belt. Then the animals were required to lick initially to receive the water reward, and each day the reward schedule was gradually dropped to 3 rewards per two meter burlap belt. Training took approximately 10 days. During imaging, mice ran on an unfamiliar cued belt, with multiple types of fabric and cues. For CA1PC imaging, we used multisensory cues, including a constant stream of pinene-scented air, a blinking ultraviolet LED, and a constant tone. For the LC imaging, since LC axons are sensitive to multisensory stimuli, and we wanted to examine signals in response to behavioral factors, these additional stimuli were not used. The mice ran three 10-minute sessions per day, separated by at least forty-five minutes. The mice were required to lick initially for the reward, and rewards were available in the location for a maximum of two seconds.

For random foraging during CA1PC recordings and LED stimulation, animals were habituated to the belt 3x for 1 day to have maximally stable place fields, then they ran 3 × 10-minute sessions per day for three days. LED stimulation began on the third session of the first imaging day, and continued for 5–6 sessions. Behavioral performance was assessed by the proportion of licks in the area immediately preceding the reward zone, beginning 35 cm before the reward.

Histology and immunohistochemistry—After the last imaging sessions mice were put under deep isoflurane anesthesia and transcardially perfused with 0.1 M PBS followed by 4% paraformaldehyde in 0.1 M PBS. After overnight post-fixation in the same solution the brains were transferred to PBS. The LC was sliced with a vibratome into 50 μm slices, while the hippocampus was sliced into 50–70 μm slices. Slices were washed 3x with 0.1 M PB, then washed in tris-buffered saline (TBS) with 0.3% triton (TBST) several times, incubated in 10% normal donkey serum in TBS for 45 minutes, then incubated for 1 hour at room temperature and for ~2 days in primary antibodies: slices were incubated with the following antibodies (for details see STAR methods): anti-GFP, anti-dsRed, or anti-Th (either chicken or rabbit). The slices were then washed with TBS several times and incubated with the appropriate secondary antibodies (see Key Resources Table). The slices were rinsed, mounted with Aquamount, and imaged on a confocal microscope.

QUANTIFICATION AND STATISTICAL ANALYSIS

Calcium imaging data preprocessing—The preprocessing steps for the raw fluorescence signal have been described elsewhere (Danielson et al., 2016). Briefly, the imaging data was motion corrected using the SIMA software package (Kaifosh et al., 2014). Frames where the motion correction failed were discarded if they were below a certain threshold of similarity to the time-averaged image of the entire calcium video. CA1PCs or LC-CA1 axons were hand-segmented using a data visualization server program developed in the lab. The same LC-CA1 axons and CA1PCs were transferred across sessions wherever possible, and identified with a unique ID, so that their activity across sessions could be tracked. Relative fluorescence changes in CA1PCs ($\Delta F/F$) were computed with a baseline calculation method adapted from Jia et al.(Jia et al., 2011), with uniform smoothing window t_1 = 3s and baseline size t_2 = 60s. For CA1PCs, we detected statistically significant

transients as described previously (Danielson et al., 2016) to use for place field calculations. More analyses were implemented using Python using custom written scripts.

For axons, the details are located in Figure S1. We first determined that the axons were synchronous by looking at the mean pairwise correlation coefficient in each session for each ROI (axon segment). A shuffle distribution of pairwise correlation coefficients was generated by taking the same axon at different sessions in time. The 99th percentile of the shuffle distribution constituted the threshold for each animal above which ROIs were included in the analyses. For each session, the remaining axons were simplified as a single trace by taking the first principal component of the signal. We finally removed any linear trends in the resulting trace over chunks of 80s of data (in case the bleaching process occurred exponentially), and smoothed using a Savitzky-Golay filter (sliding window of 21 frames, polynomial degree 6).

Place cell metrics—Detailed methods for determining statistically significant place cells and their place fields, and the enrichment of the place fields around the reward zone are described (Danielson et al., 2016; Zaremba et al., 2017). Briefly, for each CA1PC, calcium transients with onsets during running bouts of at least 1 s in duration were used to calculate the spatial information of the cell (Skaggs et al., 1993). Transients were randomly shuffled to different times during the running events, and the spatial information was recalculated. One thousand iterations were performed to create a null distribution for spatial information, and the cell was considered to be a place cell if its spatial information was above the 95^{th} percentile of the null distribution. The belt was evenly divided into 100 spatial bins, and the place field was calculated from its transient rate map over these bins. The rate map was the number of transients in a given spatial bin normalized by the animal's occupancy in that spatial bin, which was then smoothed with a Gaussian kernel (s = 3 spatial bins). To detect individual place fields, each local maximum of the smoothed rate map was fitted with a Gaussian curve centered at that location. For each smoothed rate map, the place fields where the associated Gaussian was smaller than 50% of the largest Gaussian (by measuring the total area under the curve) were discarded. The remaining Gaussians were considered place fields. The centroid of each place field was determined by the location of the peak of the Gaussian, and the location of the centroid of the largest place field was used for enrichment analysis.

Enrichment was determined by the proportion of place fields with centroids in the area beginning 25 cm before the reward zone spanning to the end of the zone. The transient frequency was calculated as the rate of significant transients detected by the method described above. The duration of the transient was taken as the beginning and end of the transient, normalized by the frame rate. The amplitude was the peak of the $\Delta F/F$ signal. For each statistically significant transient of a place cell, the area under the curve (Figure S3A) was computed as the sum of the calcium fluorescence signal during the transient duration, normalized by the frame rate.

For Figure S3C, the place cells with place fields outside the reward zone on session 1 were plotted according to the location of their centroids on subsequent sessions. Place fields within the reward zone on session 5 were plotted on previous and subsequent sessions as

well. The proportion of place cells inside the reward zone compared with cells outside the reward zone was averaged across sessions before the LED (sessions 1–4, LED off), and across sessions with the LED (Figure S3D, LED on). Recurrence probability (Figure S3B) was calculated by taking the place fields within the reward zone on day 9 in control and experimental groups, and determining the proportion of those cells that were place cells on previous days.

Generalized linear model—We use a generalized linear model to re-generate the calcium activity as a linear function of behavioral variables (Allen et al., 2017; Pinto and Dan, 2015; Turi et al., 2019). Fitting the GLM coefficients entails finding the linear combination of behavioral covariates which optimally predicts the calcium signal of LC axons. The following behavior variables were used: velocity, licking, and position. All the variables (except position) were smoothed with a Gaussian kernel (σ = 50ms). For the position signal, we divided the treadmill into 100 non-overlapping bins, which were represented in the model by 100 corresponding binary variables that were equal to one during times when the animal occupied that spatial bin and zero otherwise (Figure S1G). These behavior variables were fitted to the calcium activity using ridge regression, to manage potential collinearity of predictors and avoid overfitting.

For cross-validation, the calcium activity was divided into blocks corresponding to the number of laps in the session. We trained the model on (n-1) laps and then tested on the held-out lap. The testing lap was then rotated to cover all the n laps of the session. Finally, we concatenated all the tested laps to have the cross-validated predicted trace of the entire session. The regularization penalty was optimized separately through cross-validation on the training set, before fitting the final model on the full training set and evaluating prediction quality on the test set. To assess fit quality, we calculated the coefficient of determination (R^2) between the model's predicted axonal calcium activity and the actual axonal calcium activity. To estimate the specific contribution of each category of behavior variables, we also trained a reduced model which contained all variables except the variable of interest. We then calculated the (base-2) log-likelihood ratio between the full model and the reduced model, normalized by the number of time samples, to estimate the information gained (in bits/sample) by including the missing variable. This measure was also estimated only from the held-out test data in the cross-validation procedure.

Linear regression between speed and fluorescence signal in LC—In order to assess the amplitude of the overshoot of activity seen in the LC signal in the second phase of the goal-oriented task when the animal approaches the reward zone, we looked at the linear relationship between the velocity of the animal and the calcium trace (Figure 2G). The rationale behind this analysis is that it is impractical to estimate a baseline to generate $\Delta F/F$ values (either static or dynamic) since the activity tracks velocity (as seen in the GLM analysis, Figure 2C), and differences in $\Delta F/F$ are small. The relationship between velocity and the calcium trace was the best measure to detect changes in LC signal without altering or transforming the data to get rid of the velocity component. We computed a linear regression between the two variables in the window −35 to 0 cm before the reward, and extracted the slope of the fit.

Statistics—For all standard statistical tests (statistical details of experiments can be found in the figure legends), the a was chosen to be 0.05 for statistical significance. No statistical methods were used to predetermine sample sizes, but our sample sizes are similar to those reported in previous publications. For all the analyses, if data points followed a normal distribution (confirmed using the Kolmogorov-Smirnov test), depending on the type of comparison, a two-tailed paired sample or unpaired t-test was applied. For non-normal distributions, depending on the type of comparison, the non-parametric two-tailed paired-sample Wilcoxon signed rank test or two-tailed unpaired Mann-Whitney U test was used. If a sample had fewer than five data points, a non-parametric test was used as we did not have enough statistical power to test for normality. *, $p < 0.05$, **, $p < 0.01$, ***, $p < 0.001$. Data analysis and figures were done using custom made software in Python 2.7.15™ (https://www.python.org/).

DATA AND SOFTWARE AVAILABILITY

The data generated in this study and the analyses code will be made available upon reasonable request to the corresponding author.

Supplementary Material

Refer to Web version on PubMed Central for supplementary material.

Acknowledgments

A.L. is supported by NIMH-1R01MH100631, NINDS-1U19NS104590, NINDS-1R01NS094668, and the Kavli Foundation. A.M.K. is supported by NSF DGE-1644869 and 1F31MH117870-01A1. We would like to thank Dr. Boris Zemelman (UT Texas, Austin) for providing viruses.

References

Allen WE, Kauvar IV, Chen MZ, Richman EB, Yang SJ, Chan K, Gradinaru V, Deverman BE, Luo L, Deisseroth K, 2017 Global Representations of Goal-Directed Behavior in Distinct Cell Types of Mouse Neocortex. Neuron 94, 891–907.e6. [PubMed: 28521139]

Aston-jones G, Waterhouse B, 2016 Locus coeruleus : From global projection system to adaptive regulation of behavior. Brain Res. 1645, 75–78. [PubMed: 26969408]

Bazargani N, Attwell D, 2016 Astrocyte calcium signaling: the third wave. Nat. Neurosci. 19, 182–189. [PubMed: 26814587]

Bittner KC, Grienberger C, Vaidya SP, Milstein AD, John J, Suh J, Tonegawa S, Magee JC, 2015 Conjunctive input processing drives feature selectivity in hippocampal CA1 neurons. Nat. Neurosci. 18, 1133–1142. [PubMed: 26167906]

Bittner KC, Milstein AD, Grienberger C, Romani S, Magee JC, 2017 Behavioral time scale synaptic plasticity underlies CA1 place fields. Science 357, 1033–1036. [PubMed: 28883072]

Bouret S, Sara SJ, 2004 Reward expectation, orientation of attention and locus coeruleus-medial frontal cortex interplay during learning. Eur. J. Neurosci. 20, 791–802. [PubMed: 15255989]

Breese CR, Hampson RE, Deadwyler SA, 1989 Hippocampal Place Cells : Stereotypy and Plasticity. J Neurosci 9, 1097–1111. [PubMed: 2703869]

Breton-Provencher V, Sur M, 2019 Active control of arousal by a locus coeruleus GABAergic circuit. Nat. Neurosci. 22, 218–228. [PubMed: 30643295]

Colgin LL, Moser EI, Moser MB, 2008 Understanding memory through hippocampal remapping. Trends Neurosci.

Danielson NB, Zaremba JD, Kaifosh P, Bowler J, Ladow M, Losonczy A, 2016 Sublayer-Specific Coding Dynamics during Spatial Navigation and Learning in Hippocampal Area CA1. Neuron 91, 652–665. [PubMed: 27397517]

Dombeck D. a, Harvey CD, Tian L, Looger LL, Tank DW, 2010 Functional imaging of hippocampal place cells at cellular resolution during virtual navigation. Nat. Neurosci. 13, 1433–1440. [PubMed: 20890294]

Dupret D, O'Neill J, Pleydell-bouverie B, Csicsvari J, 2010 The reorganization and reactivation of hippocampal maps predict spatial memory performance. Nat. Neurosci. 13, 995–1002. [PubMed: 20639874]

Duszkiewicz AJ, Mcnamara CG, Takeuchi T, Genzel L, 2019 Novelty and Dopaminergic Modulation of Memory Persistence: A Tale of Two Systems. Trends Neurosci. 42, 102–114. [PubMed: 30455050]

Foote SL, Bloom FE, Aston-Jones G, 1983 Nucleus locus ceruleus: new evidence of anatomical and physiological specificity. Physiol. Rev. 63, 844–914. [PubMed: 6308694]

Fyhn M, Molden S, Hollup S, Moser M, Moser EI, 2002 Hippocampal Neurons Responding to First-Time Dislocation of a Target Object. Neuron 35, 555–566. [PubMed: 12165476]

Gauthier, Jeffrey L, Tank DW, 2018 A Dedicated Population for Reward Coding in the Hippocampus. Neuron 99, 1–15. [PubMed: 30001504]

Gauthier Jeffrey L., Tank DW, 2018 A Dedicated Population for Reward Coding in the Hippocampus. Neuron 99, 179–193.e7. 10.1016/j.neuron.2018.06.008 [PubMed: 30008297]

Glennon E, Carcea I, Martins ARO, Multani J, Shehu I, Svirsky MA, Froemke RC, 2019 Locus coeruleus activation accelerates perceptual learning. Brain Res. 1709, 39–49. [PubMed: 29859972]

Gomperts SN, Kloosterman F, Wilson MA, 2015 VTA neurons coordinate with the hippocampal reactivation of spatial experience. Elife 1–22.

Hainmueller T, Bartos M, 2018 Parallel emergence of stable and dynamic memory engrams in the hippocampus. Nature 558, 292–296. [PubMed: 29875406]

Hangya B, Ranade SP, Lorenc M, Kepecs A, 2015 Central Cholinergic Neurons Are Rapidly Recruited by Reinforcement Feedback. Cell 162, 1155–1168. [PubMed: 26317475]

Hok V, Lenck-Santini P-P, Roux S, Save E, Muller RU, Poucet B, 2007 Goal-Related Activity in Hippocampal Place Cells. J Neurosci 27, 472–482. [PubMed: 17234580]

Hollup SA, Molden S, Donnett JG, Moser M, Moser EI, 2001 Accumulation of Hippocampal Place Fields at the Goal Location in an Annular Watermaze Task. J Neurosci 21, 1635–1644. [PubMed: 11222654]

Howe M, Ridouh I, Letizia A, Mascaro A, Larios A, Azcorra M, Dombeck DA, 2019 Coordination of rapid cholinergic and dopaminergic signaling in striatum during spontaneous movement. Elife 1–24.

Howe MW, Dombeck DA, 2016 Rapid signalling in distinct dopaminergic axons during locomotion and reward. Nature 535, 505–510. [PubMed: 27398617]

Jia H, Rochefort NL, Chen X, Konnerth A, 2011 In vivo two-photon imaging of sensory-evoked dendritic calcium signals in cortical neurons. Nat. Protoc. 6, 28–35. [PubMed: 21212780]

Kaifosh P, Zaremba JD, Danielson NB, Losonczy A, 2014 SIMA: Python software for analysis of dynamic fluorescence imaging data. Front. Neuroinform. 8, 80. [PubMed: 25295002]

Kempadoo KA, Mosharov EV, Choi SJ, Sulzer D, Kandel ER, 2016 Dopamine release from the locus coeruleus to the dorsal hippocampus promotes spatial learning and memory. Proc. Natl. Acad. Sci. U. S. A. 113, 14835–14840. 10.1073/pnas.1616515114 [PubMed: 27930324]

Kentros CG, Agnihotri NT, Streater S, Hawkins RD, Kandel ER, 2004 Increased attention to spatial context increases both place field stability and spatial memory. Neuron 42, 283–295. [PubMed: 15091343]

Kobayashi T, Nishijo H, Fukuda M, Bures JAN, Ono T, 1997 Task-Dependent Representations in Rat Hippocampal Place Neurons 597–613.

Lindeberg J, Usoskin D, Bengtsson H, Gustafsson A, Kylberg A, Söderström S, Ebendal T, 2004 Transgenic expression of Cre recombinase from the tyrosine hydroxylase locus. Genesis 40, 67–73. [PubMed: 15452869]

Lovett-Barron M, Kaifosh P, Kheirbek M, Danielson N, Zaremba J, Reardon T, Turi G, Hen R, Zemelman B, Losonczy A, 2014 Dendritic inhibition in the hippocampus supports fear learning. Science 343, 857–63. [PubMed: 24558155]

Martins ARO, Froemke RC, 2015 Coordinated forms of noradrenergic plasticity in the locus coeruleus and primary auditory cortex. Nat. Neurosci. 18, 1483. [PubMed: 26301326]

McNamara CG, Tejero-Cantero Á, Trouche S, Campo-Urriza N, Dupret D, 2014 Dopaminergic neurons promote hippocampal reactivation and spatial memory persistence. Nat. Neurosci. 17, 1658–1660. [PubMed: 25326690]

Morris RGM, Garrud P, Rawlins JNP, O'Keefe J, 1982 Place navigation impaired in rats with hippocampal lesions. Nature 297, 681–683. [PubMed: 7088155]

O'Keefe J, Dostrovky J, 1971 The hippocampus as a spatial map. Preliminary evidence from unit activity in the freely-moving rat. Brain Res. 34, 171–175. [PubMed: 5124915]

O'Keefe J, Nadel L, 1978 The Hippocampus as a Cognitive Map. Oxford University Press, Oxford.

Palacios-filardo J, Mellor JR, 2019 Neuromodulation of hippocampal long-term synaptic plasticity. Curr. Opin. Neurobiol. 54, 37–43. [PubMed: 30212713]

Pinto L, Dan Y, 2015 Cell-Type-Specific Activity in Prefrontal Cortex during Goal-Directed Behavior. Neuron 87, 437–451. [PubMed: 26143660]

Rajasethupathy P, Sankaran S, Marshel JH, Kim CK, Ferenczi E, Lee SY, Berndt A, Ramakrishnan C, Jaffe A, Lo M, Liston C, Deisseroth K, 2015 Projections from neocortex mediate top-down control of memory retrieval. Nature 526, 653–659. [PubMed: 26436451]

Retailleau A, Boraud T, 2014 The Michelin red guide of the brain: role of dopamine in goal-oriented navigation. Front Syst Neurosci 8, 32. [PubMed: 24672436]

Sara SJ, Bouret S, 2012 Review Orienting and Reorienting : The Locus Coeruleus Mediates Cognition through Arousal. Neuron 76, 130–141. [PubMed: 23040811]

Skaggs WE, McNaughton BL, Gothard KM, Markus E, 1993 An Information-Theoretic Approach to Deciphering the Hippocampal Code. Adv. Neural Inf. Process. Syst. 5, 1030–1037.

Smith CC, Greene RW, 2012 CNS Dopamine Transmission Mediated by Noradrenergic Innervation. J. Neurosci. 32, 6072–6080. [PubMed: 22553014]

Stachenfeld KL, Botvinick MM, Gershman SJ, 2017 The hippocampus as a predictive map. Nat. Neurosci. 20, 1643–1653. 10.1038/nn.4650 [PubMed: 28967910]

Takeuchi T, Duszkiewicz AJ, Sonneborn A, Spooner PA, Yamasaki M, Morris RGM, Watanabe M, Smith CC, Fernández G, Deisseroth K, Robert W, 2016 Locus coeruleus and dopaminergic consolidation of everyday memory. Nature 537, 357–362. [PubMed: 27602521]

Teixeira CM, Rosen ZB, Suri D, Sun Q, Hersch M, Sargin D, Dincheva I, Morgan AA, Spivack S, Krok AC, Hirschfeld-Stoler, TessaLambe EK, Siegelbaum SA, Ansorge M, 2018 Hippocampal 5-HT Input Regulates Memory Formation and Schaffer Collateral Excitation. Neuron 98, 992–1004. [PubMed: 29754752]

Tolman EC, 1948 Cognitive maps in rats and men. Psychol. Rev. 55, 189–208. [PubMed: 18870876]

Turi G, Li W-K, Chavlis S, Pandi I, O'Hare J, Priestley JB, Grosmark AD, Liao Z, Ladow M, Zhang JF, Zemelman BV, Poirazi P, Losonczy A, 2019 Vasoactive intestinal polypeptide-expressing interneurons in the hippocampus support goal-oriented spatial learning. Neuron 101, 1–16. 10.1016/j.neuron.2019.01.009 [PubMed: 30605653]

Wagatsuma A, Okuyama T, Sun C, Smith LM, Abe K, Tonegawa S, 2018 Locus coeruleus input to hippocampal CA3 drives single-trial learning of a novel context. Proc. Natl. Acad. Sci. 115, E310–E316. [PubMed: 29279390]

Xu H, Baracskay P, O'Neill J, Csicsvari J, 2019 Assembly Responses of Hippocampal CA1 Place Cells Predict Learned Behavior in Goal-Directed Spatial Tasks on the Radial Eight-Arm Maze. Neuron 101, 119–132. [PubMed: 30503645]

Zaremba JD, Diamantopoulou A, Danielson NB, Grosmark AD, Kaifosh PW, Bowler JC, Liao Z, Sparks FT, Gogos JA, Losonczy A, 2017 Impaired hippocampal place cell dynamics in a mouse model of the 22q11.2 deletion. Nat. Neurosci. 20, 1612–1623. [PubMed: 28869582]

Ziv Y, Burns LD, Cocker ED, Hamel EO, Ghosh KK, Kitch LJ, El Gamal A, Schnitzer MJ, 2013 Long-term dynamics of CA1 hippocampal place codes. Nat. Neurosci. 16, 264–6. [PubMed: 23396101]

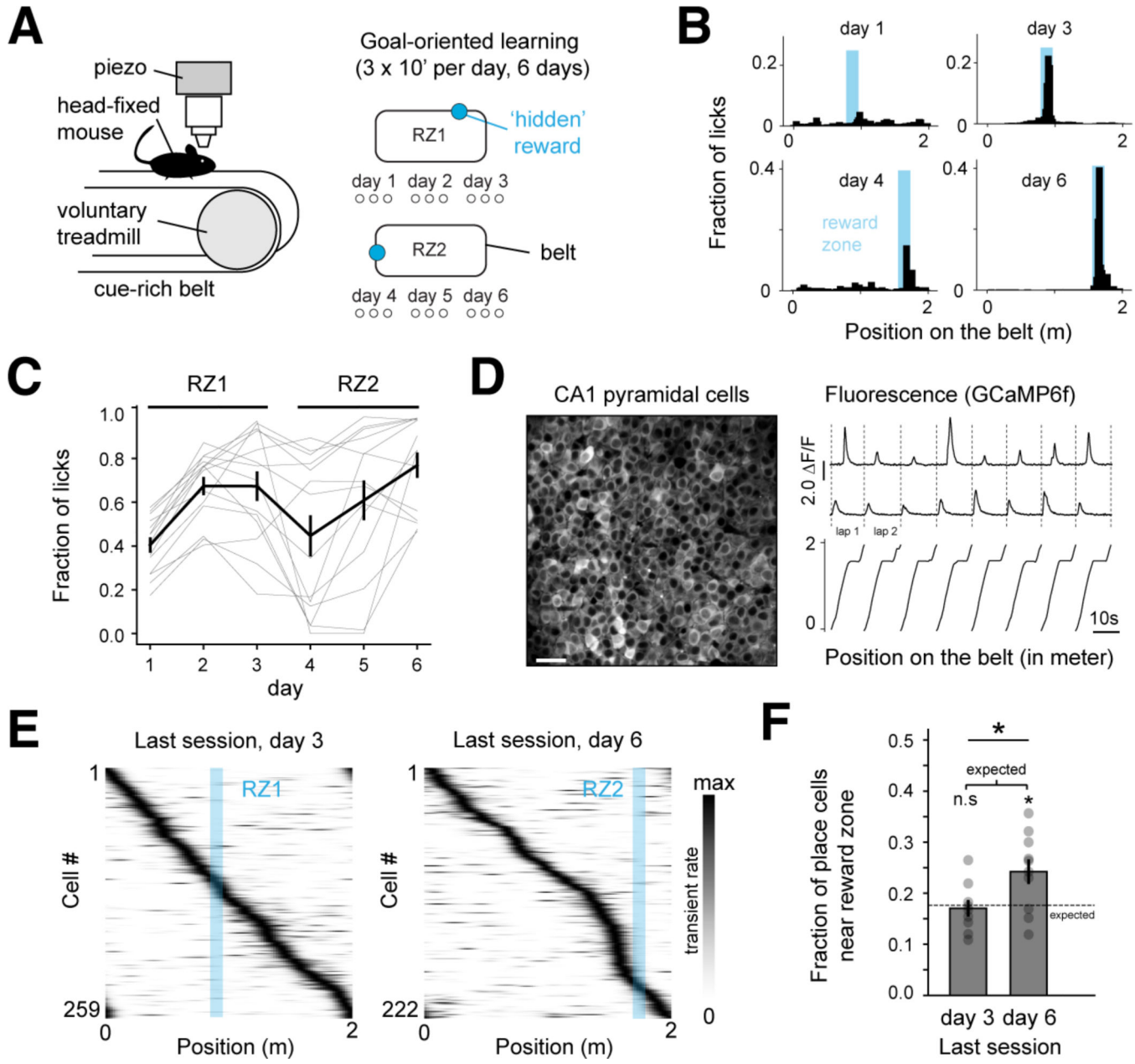

Figure 1. Place cells are enriched at a translocated reward site during GOL.

A. The goal-oriented learning (GOL) task. Mice searched for an unmarked reward zone (RZ), and water rewards were delivered operantly within the fixed 10cm zone. The RZ was at the same location for 3 days, and then moved to a new location.

B. Representative licking from one mouse. Histograms: fraction of total number of licks in each position bin (n=100). Blue shaded areas: RZs.

C. Fraction of licks within the RZ aggregated by session and plotted by day (thick line and bars: mean±SEM, thin gray lines: individual animals).

D. *Left*: time-averaged image from a representative recording session with 2p GCaMP6f imaging in CA1PCs. *Right:* relative GCaMP-calcium fluorescence ($\Delta F/F$) traces from two example place cells. Scale bar: 50 μm.

E. Example place cell tuning curves in the last session of RZ1 and RZ2. Rows: average tuning curves for individual cells along the linearized belt, normalized by peak activity. Blue shaded area: RZ location.

F. Percentage of place cells (mean±SEM) in the peri-reward zone (pRZ) defined as the RZ +25 cm preceding the zone. The last session of day6 (RZ2) shows enrichment compared with day3 (RZ1). Dashed line: percentage of place cells expected from a uniform distribution along the belt (day3: 0.17±0.045, day6: 0.242±0.07, unpaired two-tailed t-test; $t_{(18)}=-2.4$, p=0.02. One-sample two-tailed t-test for expected value derived from the uniform distribution; day3: $t_{(8)}=-0.36$, p=0.72, day 6: $t_{(9)}= 2.72$, p=0.02).

See also Figures S2–4.

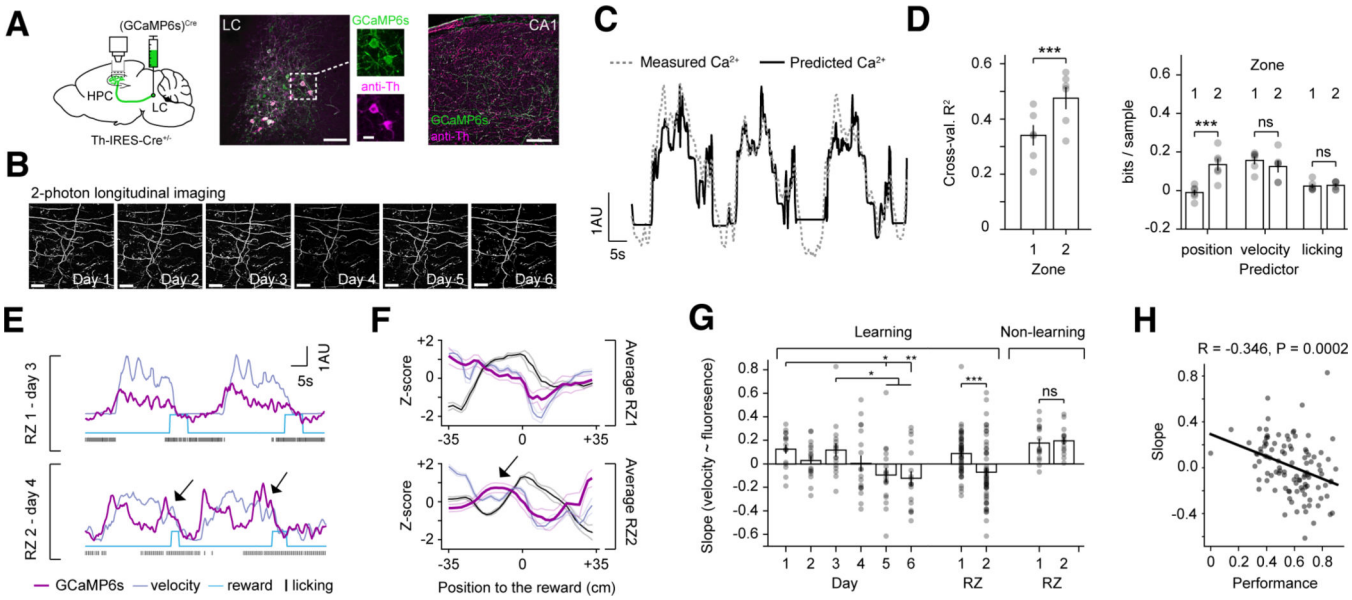

Figure 2. Locus coeruleus activity changes during GOL

A. *Left:* LC-CA1 axon labeling strategy. Cre-dependent virus [rAAV2/9:EF1a-(GCaMP6s)^{Cre}] was injected into the locus coeruleus (LC) of Th-IRES-Cre$^{+/-}$ mice. LC axons in hippocampal (HPC) CA1 were imaged through a cannula. *Middle* and *right*: post hoc immunofluorescent staining with antibodies against tyrosine-hydroxylase (anti-Th) and GCaMP (anti-GFP) in LC and HPC to confirm labeling strategy. Scale bar: LC: 50 μm; inset: 20μm, HPC: 100 μm.

B. Example of multi-day 2p imaging of LC-CA1 axons in CA1 stratum oriens (SO). Scale bar: 50 μm.

C. A generalized linear model (GLM) trained with three covariates (position, velocity, and licking) to predict LC-CA1 activity. Example trace of LC-CA1 calcium activity (dashed line) and predicted by the GLM (solid line).

D. *Left*: cross-validated R^2 calculated on the held out test data in RZ1 sessions and RZ2 sessions (mean±SEM, RZ1: 0.34±0.04; RZ2: 0.48±0.04; n=6 mice, two-tailed paired t-test, $t_{(5)}$=−5.97, p=0.004). *Right*: contribution of different variables estimated by the amount of information gained by including each variable during RZ1 and RZ2 (mean±SEM; position in RZ1: −0.01±0.013; position in RZ2: 0.14±0.03; velocity in RZ1: 0.15±0.03; velocity in RZ2: 0.12±0.03; licking in RZ1: 0.02±0.01; licking in RZ2: 0.03±0.01; n=6 mice, two-tailed paired t-tests between RZ1 and RZ2 for: velocity, $t_{(5)}$=−4.84, p=0.005; position, $t_{(5)}$=1.49, p=0.196; licking, $t_{(5)}$=−0.63, p=0.556).

E. Example traces of LC-CA1 activity (dark magenta) and behavioral variables in RZ1 and RZ2 for 2 consecutive laps. In RZ1, axons are correlated with velocity, while in RZ2, there is a decorrelation between LC-CA1 activity and velocity (arrows). 1 arbitrary unit (AU) refers to 1 sigma of the Z-score trace for the fluorescence *F*(GCaMP6s), and speed in cm/s (velocity).

F. Average peri-stimulus activity histogram of the LC-CA1 signal (dark magenta), velocity (lavender) and licking (black) in RZ1 and RZ2, centered around reward. The overshoot in

LC-CA1 activity is only visible in RZ2 (arrow) (n=6 mice, mean: darker colors, SEM: lighter colors). It preceded the reward by an average of 24.33±2.02 cm.

G. Slope of the linear fit between velocity and LC-CA1 signals. The signals are less correlated over the course of learning. Data are in mean±SEM for sessions in a given day collected from n=6 mice (Learning day1: 0.126±0.038; day2: 0.03±0.036; day3: 0.118±0.056; day4: 0.006±0.067; day5:−0.093±0.061; day6:−0.121±0.059. One-way mixed-effects model ANOVA $F_{(5, 82)}$=4.28, p=0.0017. Post-hoc Tukey test, day1 vs. day5, p=0.026. day1 vs. day6, p=0.008. day2 vs. day5, p=0.047. day2 vs. day6, p=0.016), and are correlated in RZ1 but decorrelated in RZ2 (Learning RZ1: 0.09±0.026; RZ2: −0.069±0.036. Two-tailed unpaired t-test, n_1=51 sessions, n_2=54 sessions, $t_{(104)}$=−3.57, p=0.0005). Two mice that did not learn the task showed signals correlated with velocity in both RZs (Non-learning RZ1: 0.175±0.037, RZ2: 0.194±0.03. Two-tailed unpaired t-test, n_1=15 sessions, n_2=16 sessions, $t_{(30)}$=0.399, p=0.693).

H. The slope of the relationship between speed and fluorescence was correlated with behavioral performance, as measured by the fraction of licks in the RZ (Pearson's R test, n=105 points, R=−0.346, p=0.0002). Each point is the average performance as a function of the average correlation coefficient for each session, and each mouse.

See also Figures S1–4.

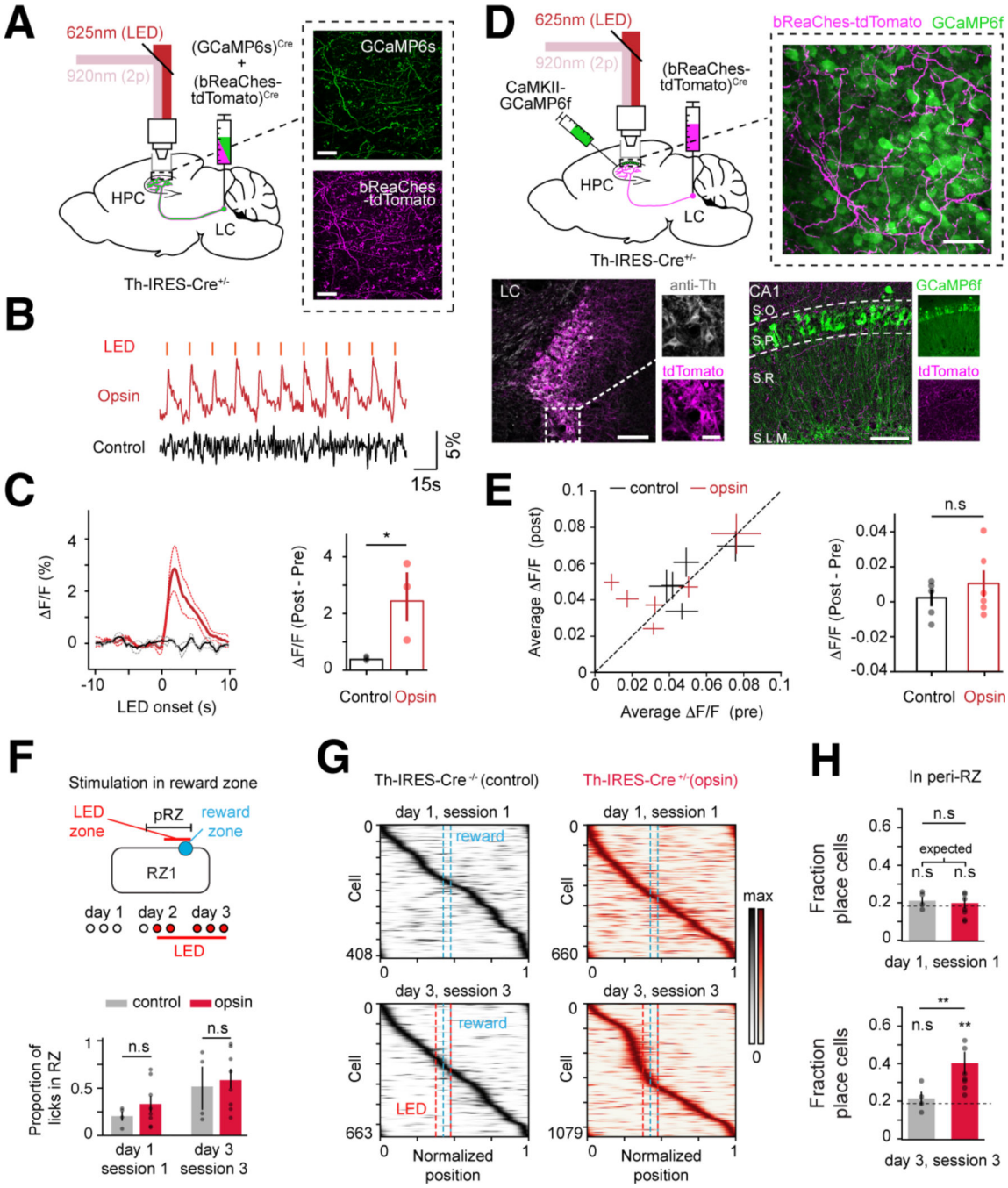

Figure 3. Stimulating LC-CA1 axons induces CA1 place cell enrichment near a rewarded location during GOL.

A. *Left*: labelling strategy for optogenetic stimulation and imaging of LC-CA1 axons. The LC was injected with rAAV2/9:EF1a-(GCaMP6s)^{Cre} and rAAV2/9:EF1a-(bReaChes-tdTomato)^{Cre}. *Right*: time-averaged 2p images of GCaMP6s and bReaChes-tdTomato in CA1 *in vivo,* showing overlap between the two. Scale bar: 50 μm.

B. Δ*F/F* traces of LC-CA1 axons expressing either GCaMP6s and bReaChes (opsin), or GCaMP6s only (control). Photostimulation: 1s pulse every 20s.

C. *Left*: average $\Delta F/F$ traces in control and opsin mice, (n=3 mice per condition). Dotted line: SEM. *Right*: difference of $\Delta F/F$ between post and pre stimulation was higher for opsin mice (mean±SEM, control: $2\times10^{-4}\pm4\times10^{-4}$; opsin: 0.0246±0.008. Two-tailed unpaired t-test, $t_{(5)}=-2.9$, p=0.044).

D. *Top left*: labelling strategy for optogenetic stimulation of LC-CA1 axons and imaging of CA1PCs. rAAV2/9:EF1a-(bReaChes-tdTomato)^{Cre} was injected in the LC, and rAAV2/1:CaMKII-GCaMP6f was injected in CA1. *Top right:* averaged 2p Z-stack of CA1PCs and LC-CA1 axons. Scale bar: 50 μm. *Bottom left*: example LC injected with bReaChes-tdTomato and stained for tyrosine hydroxylase (anti-Th). *Bottom right*: example HPC stained for td-Tomato. LC-CA1 axons labelled with bReaChes-tdTomato can be seen in all layers (S.O.: *stratum oriens*, S.P.: *str. pyramidale*, S.R.: *str. radiatum*, S.L.M.: *str. lacunosum-moleculare*). Scale bars: LC and CA1,100 μm; LC inset, 20 μm.

E. Stimulating LC-CA1 axons does not acutely affect CA1PC activity. Difference in $\Delta F/F$ during pre- vs. post-light stimulation. *Left*: each cross is one mouse, size of the cross is SEM. *Right*, average difference post- minus pre-light stimulation (mean±SEM, control: 0.0015±0.0047, opsin: 0.0097±0.0075. Two-tailed unpaired t-test, $t_{(11)}=0.88$, p=0.403; control, n=5 mice; opsin, n=6 mice). Red: Th-IRES-Cre$^{+/-}$ mice injected with bReaChes-tdTomato in the LC (opsin), black: Th-IRES-Cre$^{-/-}$ (control). Each dot is one mouse.

F. *Top*: optogenetic stimulation of LC-CA1 axons in RZ1 of the GOL task. The LED stimulation began 10cm before reward and spanned the whole RZ. The peri-reward zone (pRZ) began 25cm before the LED zone. *Bottom*: opsin (Th-IRES-Cre$^{+/-}$, n=8 mice) and control (Th-IRES-Cre$^{-/-}$, n=4 mice) animals showed the same behavioral learning dynamics (mean±SEM, session1, control: 0.203±0.048; opsin: 0.332±0.083. session9, control: 0.514±0.182; opsin: 0.583±0.108. Mann-Whitney U test. session1, $z_{(11)}=12.0$, p=0.28, session 9, $z_{(11)}=12.0$, p=0.28).

G. Heatmaps of place cells in the first and last sessions of control and opsin mice. Opsin mice show a large degree of enrichment before the light stimulation zone in the last session (session9).

H. Percentage of place fields in the peri-reward zone (pRZ) in session1 (top) and session9 (bottom). Session9 of opsin mice shows enrichment compared with control (mean±SEM, session1, control: 0.216±0.019; opsin: 0.199±0.028. session9, control: 0.216±0.035; opsin: 0.402±0.059. Mann-Whitney U test. Session1, $z_{(11)}=12.0$, p=0.276, session9, $z_{(11)}=3.0$, p=0.017. Session1, control vs. expected distribution: $t_{(3)}=1.3$, p=0.28; opsin vs. expected distribution: $t_{(7)}=1.21$, 0.26. session9, control vs. expected $t_{(3)}=1.95$, p=0.14; opsin vs. expected: $t_{(7)}=4.11$, 0.004).

See also Figure S4.

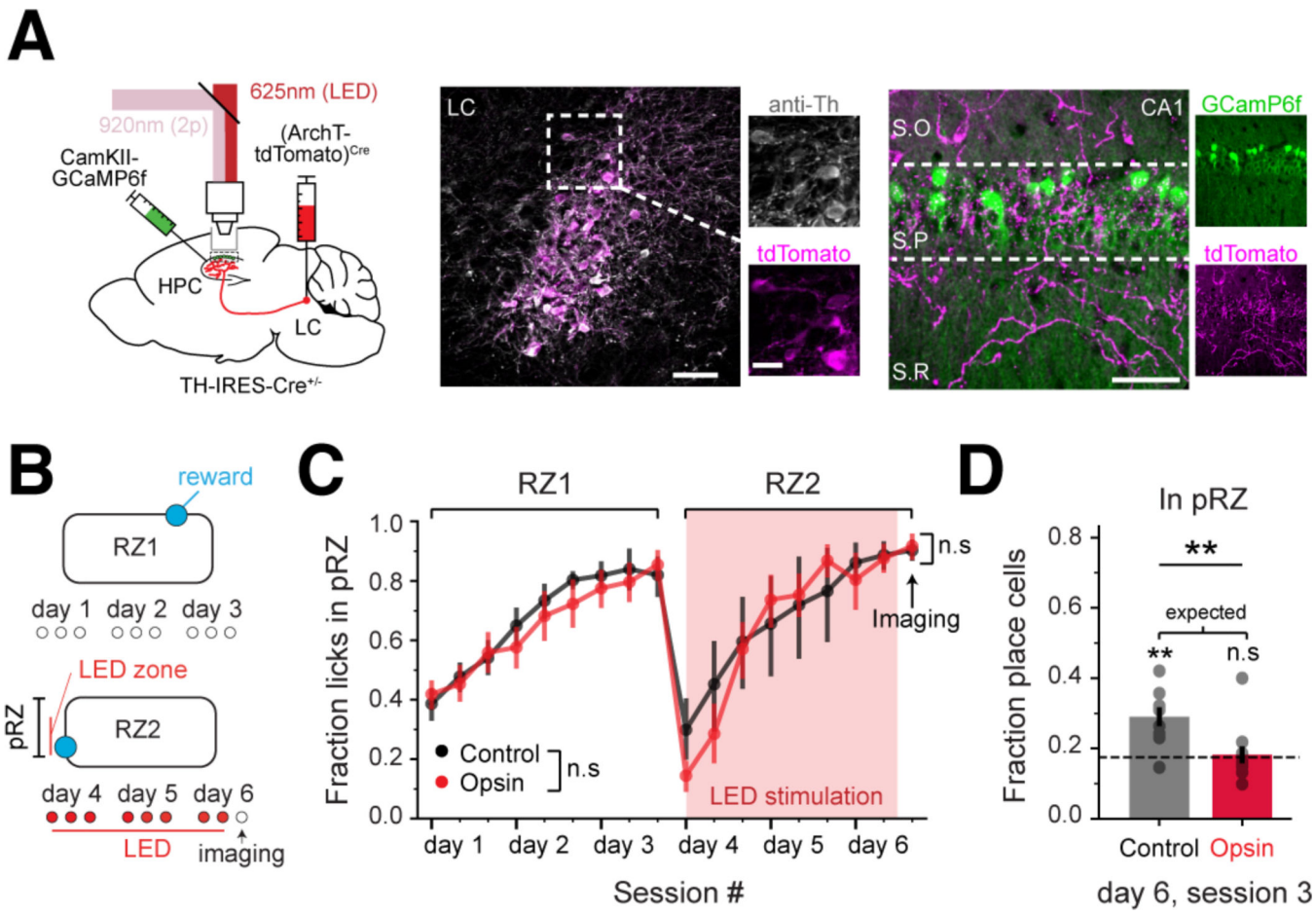

Figure 4. Inhibition of LC-CA1 axons decreases CA1 place field enrichment

A. *Left*: labelling strategy for LC-CA1 optogenetic inhibition and imaging of CA1PCs. The LC was injected with rAAV2/9:EF1a-(ArchT-tdTomato)^{Cre} and rAAV2/1:CaMKII-GCaMP6f was injected in CA1. *Middle*: example LC injected with ArchT-tdTomato and stained for tyrosine hydroxylase (anti-Th). *Right*: example HPC section. LC-CA1 axons labelled with ArchT-tdTomato can be seen in all layers. Scale bars: LC and CA1: 50 μm; LC inset: 20μm.

B. Optogenetic inhibition of LC-CA1 axons started on the session1 of RZ2 of the GOL task. The LED stimulation zone began 10cm before the reward and spanned the whole RZ.

C. *Left:* opsin (Th-IRES-Cre$^{+/-}$, n=11 mice) and control (Th-IRES-Cre$^{-/-}$, n=9 mice) animals showed the same behavioral learning dynamics (mean±SEM, repeated measures ANOVA, opsin vs. control, within-subject factor of session, $F_{1,17}$ =1.89, p=0.17). Opsin and control mice showed the same behavioral performance in the last session of RZ2 (unpaired two-tailed t-test, $t_{(19)}$=0.35, p=0.72).

D. Percentage of place cells in the peri-reward zone (pRZ) for control and opsin mice (mean ±SEM). Dashed line: percentage of place cells expected from a uniform distribution (expected=0.176. control: 0.29±0.03, opsin: 0.18±0.02. Opsin vs. control, unpaired two-tailed t-test, $t_{(19)}$=3.02, p=0.007. One-sample two-tailed t-test for expected value, control: $t_{(8)}$=4.32, p=0.003, opsin: $t_{(10)}$=0.28, p=0.77).

KEY RESOURCES TABLE

REAGENT or RESOURCE	SOURCE	IDENTIFIER
Antibodies		
Anti-GFP, chicken, 1:500–1:1000	Abcam	ab13970
Anti-dsRed, rabbit, 1:1000	Takara	632496
Anti-Th, chicken, 1:500	Abcam	ab76442
Anti-Th, rabbit, 1:100	Millipore	AB152
anti-chicken Alexa 488, 1:300	Jackson	703-545-155
Anti-chicken Alexa 647, 1:300	Jackson	703-605-155
Anti-rabbit Alexa 568, 1:300	Abcam	ab175692
Anti-rabbit Alexa 647, 1:300	Jackson	711-605-152
Bacterial and Virus Strains		
rAAV2/1:EF1α-(GCaMP6s)^{Cre}	Boris Zemelman	N/A
rAAV2/1:EF1α-(ArchT-tdTomato)^{Cre}	Boris Zemelman	N/A
rAAV2/9:EF1α-(bReaChES-tdTomato)^{Cre}	Boris Zemelman	N/A
rAAV2/1:Syn-GCaMP6f	This paper	Addgene virus 100837-AAV1
rAAV2/1:CamKII-GCaMP6f	This paper	Addgene virus 100834-AAV1
Chemicals, Peptides, and Recombinant Proteins		
PBS	Thermo Fisher	7732-18-5
PFA	Electron Microscopy Sciences	15714-S
Triton X-100	Sigma-Aldrich	T8787-100ML
Normal Donkey serum	Jackson Immuno	017-000-121
Aquamount	Fisher Scientific	14-390-5
Deposited Data		
Analyzed data	This paper	N/A
Experimental Models: Organisms/Strains		
Th-IRES-Cre	Lindeberg et al., 2004, from Dr. Eric Kandel	N/A
VIP-IRES-cre	The Jackson Laboratory	010908
Th-IRES-Cre × VIP-IRES-Cre	this paper	N/A
Software and Algorithms		
Python 2.7.15	www.python.org	N/A
SIMA	Kaifosh et al., 2014	https://github.com/losonczylab/sima